Accepted for publication in PASP [2 Dec 2010]

The Ohio State Multi-Object Spectrograph

Paul Martini[1], Rebecca Stoll, M.A. Derwent, R. Zhelem, B. Atwood, R. Gonzalez, J.A. Mason, T.P. O'Brien, D.P. Pappalardo, Richard W. Pogge[1], B. Ward, M.-H. Wong

Department of Astronomy, The Ohio State University, 140 West 18th Avenue, Columbus, OH 43210, USA

ABSTRACT

The Ohio State Multi-Object Spectrograph (OSMOS) is a new, wide-field imager and multi-object spectrograph for the 2.4-m Hiltner Telescope at the MDM Observatory. OSMOS has an all-refractive design that reimages a 20 arcminute diameter field-of-view onto the 4064x4064 MDM4K CCD with a plate scale of 0.273 arcseconds per pixel. Approximately an $18.5'$ square region of this field illuminates the detector and is available for spectroscopy, although with reduced wavelength coverage near the edges of the field. Slit masks, filters, and dispersers are all mounted in a series of six-position aperture wheels. These mechanisms rotate between positions in only a few seconds and consequently the instrument may be rapidly reconfigured between imaging and spectroscopic modes. At present a low-resolution triple prism ($R \sim 60 - 400$) and a moderate resolution VPH grism ($R \sim 1600$) are available.

Subject headings: instrumentation: spectrographs

1. Introduction

The Ohio State Multi-Object Spectrograph (OSMOS) provides a new wide-field imaging and multi-object spectroscopic capability at the 2.4m Hiltner telescope of the MDM Observatory. Multi-object spectroscopy is relatively rare at small to moderate aperture telescopes (< 6m diameter), although notable exceptions exist such as the multi-slit WFCCD spectrograph at Las Campanas and fiber-fed multi-object spectrographs such as the Sloan Digital Sky Survey Spectrographs at Apache Point Observatory (Uomoto et al. 1999) and the Hydra Spectrograph at the WIYN telescope. Moderate aperture telescopes can readily obtain spectra of 19–20 mag objects and, provided the target surface density is sufficiently high, can provide substantial efficiency gains from multiplexing.

[1]Center for Cosmology and Astroparticle Physics, 191 West Woodruff Avenue, Columbus, OH 43210

One of the key science motivations for the construction of OSMOS was the study of galaxies in groups and clusters in the nearby universe. These sources represent substantial overdensities of relatively bright $R < 20$ mag galaxies on tens of arcminute scales and are ideally suited for study with multi-object spectrographs on moderate-aperture telescopes. Studies of nearby groups and clusters with substantial spectroscopic data have led to important insights into the physical processes that affect galaxy evolution (e.g. Dressler 1980; Dressler et al. 1987; Djorgovski & Davis 1987; Zabludoff & Mulchaey 1998). Spectroscopic observations of X-ray sources in the fields of groups and clusters to identify Active Galactic Nuclei (AGN) have also provided new information about AGN demographics and the extent to which physical processes on the group and cluster scale also accretion onto supermassive black holes (e.g. Martini et al. 2006, 2009).

Another motivation for OSMOS was the capability to obtain both wide-field images and long-slit spectroscopy in relatively rapid succession. The science driver for this capability is the study of transient objects, in particular gamma-ray bursts and supernovae (e.g. Stanek et al. 2003). A multi-purpose instrument such as OSMOS is well-suited to 'interrupt mode' observations of such objects because it may be rapidly reconfigured. In addition, many small to moderate aperture telescopes, such as the Hiltner telescope, may only have one instrument mounted at a time. Because the multi-purpose nature of OSMOS should make it attractive to a substantial fraction of the user community, OSMOS is more likely to be mounted on the telescope when observations of transient objects are desired. Finally, the multi-purpose nature also facilitates queue-scheduled observations of more long-term time-domain targets that may only require observations for a fraction of a night on a regular basis, such as microlensing in lensed QSOs (e.g. Morgan et al. 2006) and reverberation mapping of broad-line AGN (e.g. Peterson et al. 2004). All of these considerations motivated our design of OSMOS and we built this instrument with the goal that it will become a facility wide-field imager and spectrometer on the MDM 2.4m telescope.

2. Optical Design

OSMOS was designed for use with the f/7.8 focus of the 2.4-m Hiltner telescope at the MDM Observatory. The Hiltner telescope is approximately a Ritchey-Chrétien design and delivers a scale of $11.528''\mathrm{mm}^{-1}$. The focal surface is well-approximated by a sphere with a 1263mm radius of curvature that is concave toward the secondary.

The requirement for wide-field, multi-object spectroscopy, as well as interest among MDM consortium members for a new, general-purpose spectrograph and wide-field imager, led to an exploration of all-refractive designs. The model for OSMOS was the WFCCD instrument at the 2.5-m du Pont telescope at Las Campanas Observatory. The WFCCD has a range of low-resolution grism options for both long-slit and multi-object spectroscopy over a $25'$ diameter field of view. OSMOS was designed to mount to the Hiltner telescope's Multi-Instrument System (MIS). The MIS contains a guider module and a calibration lamp system employed by the majority of MDM instruments, including OSMOS. The maximum unvignetted field-of-view (FOV) of the MIS is a $20'$

diameter circle and OSMOS was consequently designed for this field size. A further constraint was the decision to use the existing MDM4K detector system[1], which is a 4064×4064 array with 15μm pixels. This device was thinned and packaged by the University of Arizona Imaging Technology Laboratory. Ohio State mounted this CCD in a Dewar and built the controller electronics (Head Electronics, hereafter HE). This device has a standard broadband anti-reflection coating. The peak quantum efficiency is nearly 90% at 600nm and above 60% from 300–850nm.

2.1. Collimator and Camera

The OSMOS collimator is an f/7.8 double-Gauss design with a 14 degree FOV and contains a total of five lenses, including a doublet. The optical design is shown in Figure 1 and the optical prescription is provided in Table 1. The first collimator element is approximately 70mm from the telescope focal surface, which provides ample space for the slit wheel. The collimated beam diameter is 55mm and the pupil is located 70mm from the vertex of the last collimator element. The total collimated beam space is 170mm. This allows room for a relatively large triple prism for ultra-low-resolution spectroscopy, the significant prism angles required to produce moderate-resolution VPH grisms, and a pair of filter wheels.

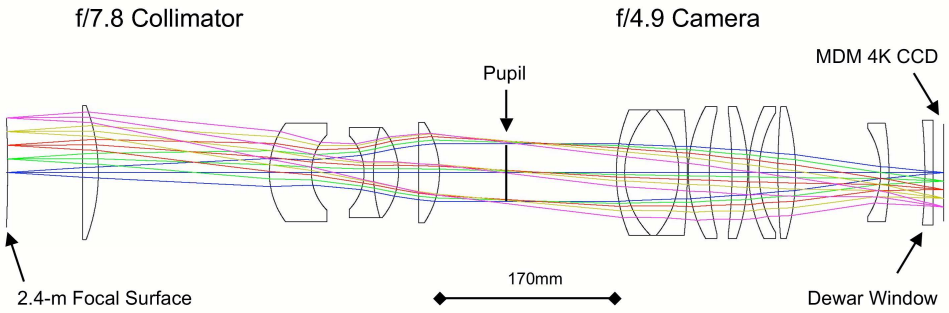

Fig. 1.— Optical design with ray traces for field angles up to 10′ off axis. Light enters the instrument from the left. The first surface corresponds to the curved focal surface of the 2.4-m Hiltner telescope. This is the location of the slit wheel in the optical path. The disperser and two filter wheels are in the collimated beam space near the pupil. The last lens on the right is the Dewar window of the MDM4K detector system. The optical prescription is provided in Table 1.

The camera is an f/4.9 Petzval design with an 18 degree FOV. This FOV is larger than the 14 degree FOV of the collimator to allow dispersed light into the corners of the detector. The detector ultimately limits the wavelength range observed for objects near the edges of the FOV.

[1]See http://www.astronomy.ohio-state.edu/~jdeast/4k/ for a complete description of this system.

Table 1. Optical Prescription

Lens	Surface	Radius	Thickness	Material	Diameter
FOC	0	-1263.00	70.0		140.
COL-1	1	0.00	15.0	BSL7Y	128.
	2	-180.89	164.0		128.
COL-2	3	78.80	40.3	BSM51Y	94.
	4	50.68	50.5		72.
COL-3	5	-50.68	9.0	BAL15Y	70.
COL-4	6	152.30	24.0	CAF2	86.
	7	-67.25	19.3		86.
COL-5	8	0.00	20.0	CAF2	96.
	9	-86.26	169.6		96.
CAM-1	10	152.72	8.0	BSM51Y	120.
CAM-2	11	84.60	52.0	CAF2	120.
CAM-3	12	-93.70	8.0	BSM51Y	120.
	13	-624.50	1.0		120.
CAM-4	14	127.30	20.0	CAF2	126.
	15	231.77	22.0		116.
CAM-5	16	-468.30	15.0	BAL15Y	116.
	17	-188.69	1.0		126.
CAM-6	18	143.25	10.0	BSM51Y	126.
	19	111.40	18.0		114.
CAM-7	20	751.20	17.0	SILICA	126.
	21	-222.21	81.5		126.
CAM-8	22	-77.85	8.0	S-LAL7	84.
	23	-311.32	34.4		94.
CAM-9	24	-523.76	8.0	SILICA	100.
	25	0.00	10.0		100.

Note. — Optical prescription for OSMOS. All dimensions are in mm. The row labeled FOC corresponds to the focal surface of the 2.4m Hiltner telescope. Long slits and multi-object slit masks are designed to have this radius of curvature. The CAM-9 lens is the window of the MDM4K CCD Dewar. The camera optical design was constrained to be compatible with this lens.

The camera contains a total of 9 lenses, including a triplet. One of these nine lenses is the window of the MDM4K Dewar, which was designed to have mild curvature. The optical design produces a final plate scale of $0.273''$/pixel on the MDM4K. This plate scale is reasonably well matched to the typical image quality obtained at the site. The spectroscopic modes described below were designed for use with a $1''$ wide slit. The unvignetted FOV is a $20'$ diameter circle and the central $18.5' \times 18.5'$ illuminates the MDM4K.

We chose to purchase complete lens barrel assemblies for both the collimator and camera in order to save development and assembly time. Separate lens barrel assemblies for the collimator and camera were purchased from Coastal Optical Systems (now Jenoptik Optical Systems) in Jupiter, FL. Both the collimator doublet and the camera triplet contain bonds of Calcium Fluoride to optical glasses (BAL15Y and BSM51Y). These materials have substantial differences in their coefficients of thermal expansion. We therefore specified that these lenses should be bonded with Sylgard 184, a silicone encapsulant most commonly used in electronics components, yet which also has excellent visible-wavelength transmission and retains some pliability when cured. Sylgard 184 has been used in a number of other astronomical instruments, such as the MIKE spectrograph at the 6.5m Magellan Clay telescope (e.g. Bernstein et al. 2003) and the SOAR Optical Imager[2].

Figure 2 demonstrates the predicted image quality expressed as the FWHM in arcseconds as a function of field angle in the $UBVRI$ bandpasses. The 80% encircled energy diameter (D80) in monochromatic light is 10μm. At the optimum polychromatic focus, D80 varies between 10μm and 30μm between 370 and 1000nm. These variations are minor relative to the expected site image quality and a single focus is suitable for all wavelengths. D80 in polychromatic light is 20μm or $0.36''$ on axis. The temperature dependence of the best focus is 350μm per 10 degrees Celsius. As a consequence, some seasonal variation in the best camera focus position is expected. A temperature sensor is attached to the optical bench so that this correction could be automated in the future.

2.2. Dispersers

OSMOS was designed to employ grisms, in particular ones that contain Volume Phase Holographic (VPH) gratings, as well as an ultra-low dispersion prism. The main requirement on the final size of the large collimated beam space was clearance for a triple prism disperser (see Figure 3). The triple prism contains a pair of S-FPL51Y prisms with $\phi = 28.5^\circ$ apex angles that sandwich a PBM2Y prism with a $\phi = 45^\circ$ apex angle. This design is zero deviation. The triple prism produces ultra-low and variable resolution of $R = 400 - 60$ (for 400–1000nm with a $0.9''$ slit) at very high efficiency. The triple prism was also fabricated by Jenoptik Optical Systems. A photograph of the triple prism is shown in Figure 3 and the resolution as a function of wavelength is shown in Figure 4.

[2]http://www.soartelescope.org/observing/documentation/soar-optical-imager-soi/

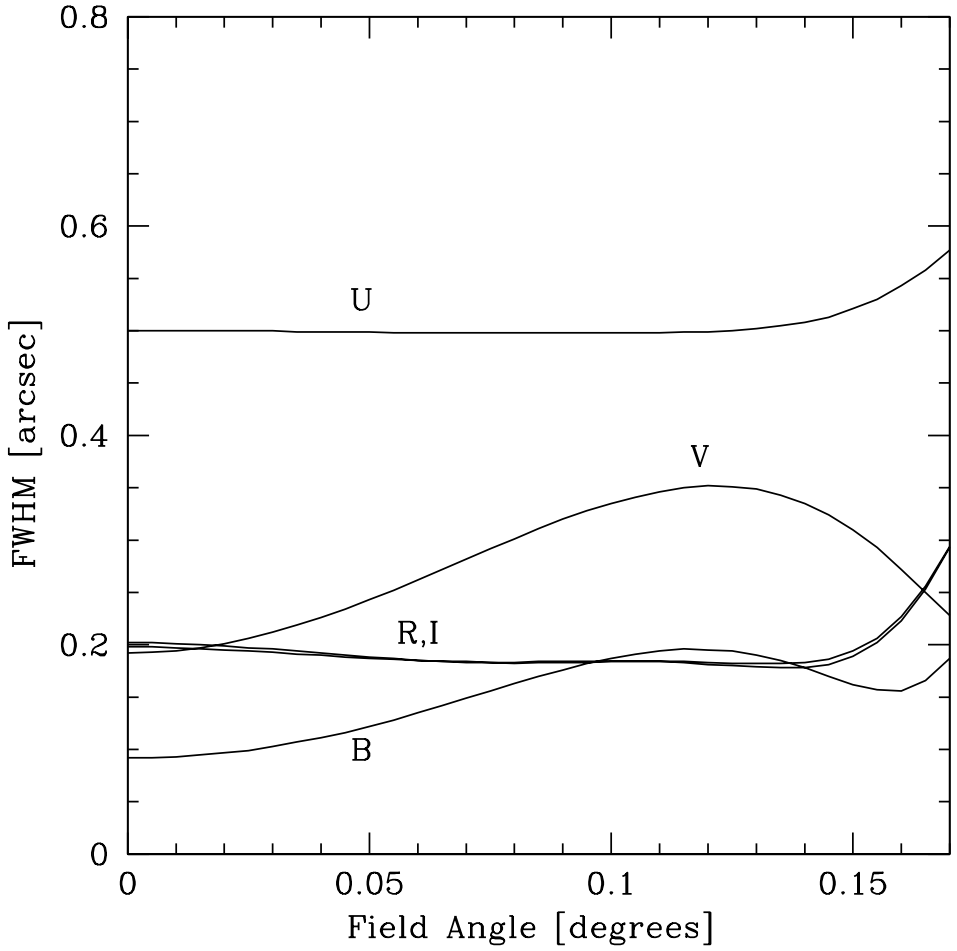

Fig. 2.— FWHM in arcseconds as a function of off-axis angle for five representative broad-band filters. One pixel corresponds to 0.273″ and the maximum unvignetted field is 10′ (0.167°).

The first VPH grism purchased for OSMOS was designed to produce $R = 1600$ resolution with a 1″ wide slit. The peak diffraction efficiency (Blaze wavelength) was designed to be at $\lambda_B = 450$nm for a long slit at the center of the field. These specifications were achieved with a $\rho = 704$ lines/mm VPH grating sandwiched between a pair of BSL7Y prisms with $\phi = 17°$ apex angles. The grating fringes are normal to the grating surface. We designed the grating with the aid of software tools kindly made available by Gary Bernstein on his website[3]. A grism with these parameters was purchased from Kaiser Optical Systems in Ann Arbor, MI. The measured peak efficiency of the purchased grating was 92%.

[3]http://www.physics.upenn.edu/~garyb/

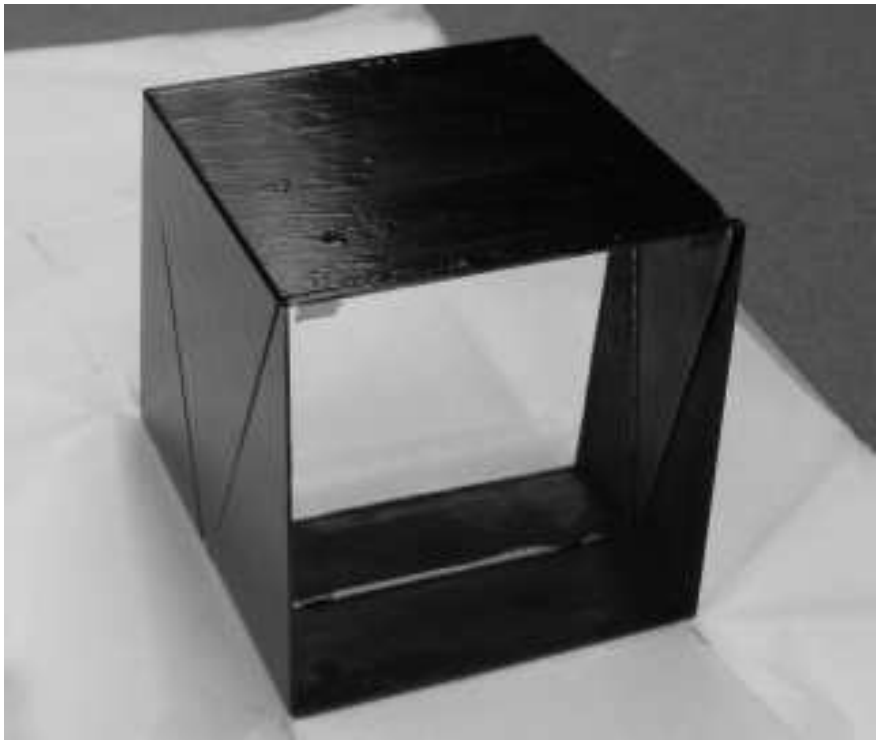

Fig. 3.— Photograph of the triple prism upon its arrival in Columbus, OH. The prism consists of a PMB2Y prism sandwiched between two, identical S-FPL51Y prisms. The height and width of the prism are 84mm and the base is 97.5mm along the optical axis. See Section 2.2 for further details.

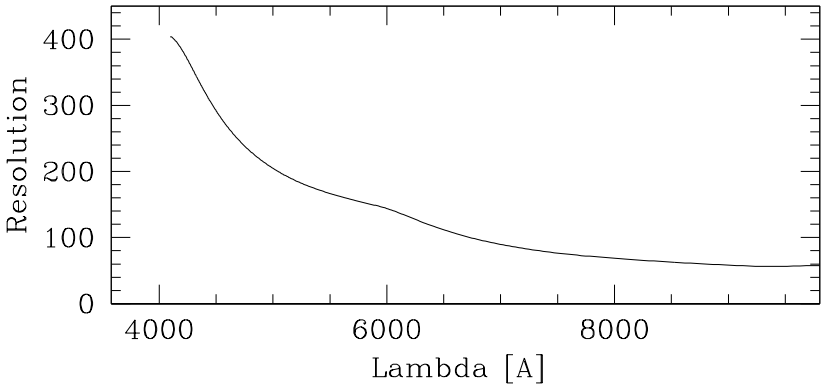

Fig. 4.— Resolution of the triple prism as a function of wavelength for a 0.9″ wide slit. See Section 2.2 for further details.

One important, generic property of VPH gratings is that their peak diffraction efficiency is a function of the incident angle relative to the fringes (Barden et al. 2000). The peak diffraction

efficiency is shifted in wavelength for rays that do not enter the grating at the blaze angle. There is also some net loss of efficiency, although the efficiency at wavelengths in the vicinity of the (shifted) peak may be higher than achieved for rays at the blaze angle. The full range of incident angles in OSMOS is ± 7 deg and this range allows some 'tuning' of the peak diffraction efficiency with the use of non-centered long slits. We designed long-slit cells that can position a slit $\pm$30mm ($\pm 6'$) relative to a centered slit. The corresponding predicted wavelength shifts of these off-center slits are approximately +150nm ($+6'$) and $-$70nm ($-6'$). The predicted relative diffraction efficiencies at these three field angles are shown in Figure 5.

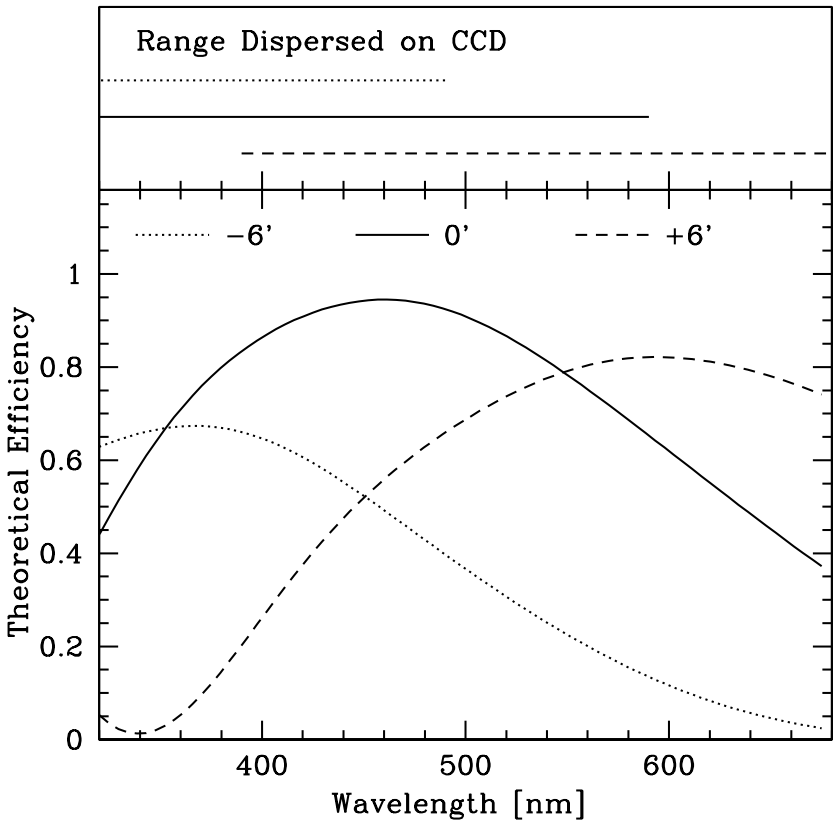

Fig. 5.— Predicted diffraction efficiency for the $R = 1600$ VPH grism at three field positions: on axis (*solid line*), $+6'$ (*dashed line*), and $-6'$ (*dotted line*). Positive field angles correspond to rays with smaller incidence angles on the grating substrate than an on-axis ray. The measured peak diffraction efficiency of the grating on axis is 92%, or approximately 5% less than the theoretical value shown. Only one polarization is shown for clarity (perpendicular to the plane of incidence). The other polarization is nearly identical. The upper panel illustrates the wavelength range dispersed on the detector.

3. Mechanical Design

OSMOS has a total of six mechanisms: four six-position aperture wheels (slit, disperser, and two filters wheels) and two linear focus stages for the collimator and camera lens barrels. Figure 6 is a solid model of the instrument and Figure 7 shows a photograph of the interior that indicates the positions of the mechanisms. In the first two subsections below we briefly describe the design and performance of the aperture wheels and linear mechanisms. Further details were presented in Stoll et al. (2010). The following subsection describes the mechanical design and expected performance of the optical bench and enclosure.

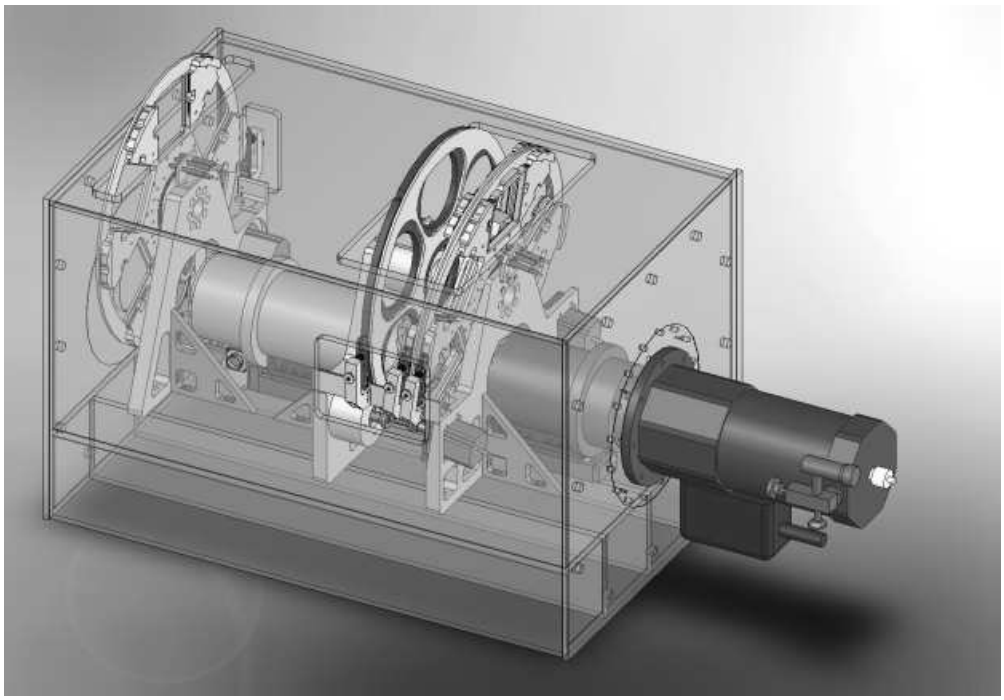

Fig. 6.— Solid model of OSMOS and the MDM4K detector system. Light enters the instrument from the left. The first aperture wheel is the slit wheel. The collimator and camera lenses are mounted in the barrels as shown, while the disperser wheel and filter wheels cross the optical path between them in the collimated beam space. The two filter wheels are tilted by 8° relative to the optical axis to mitigate ghost reflections.

3.1. Aperture Wheels

The four aperture wheels are the third generation of a design originally developed for 12-position filter wheels at the 1.3-m McGraw-Hill Telescope at the MDM Observatory and the 1-m Yale Telescope at the Cerro Tololo Inter-American Observatory. The second generation is the Multi-Object Double Spectrograph (MODS) for the Large Binocular Telescope (Pogge et al. 2006).

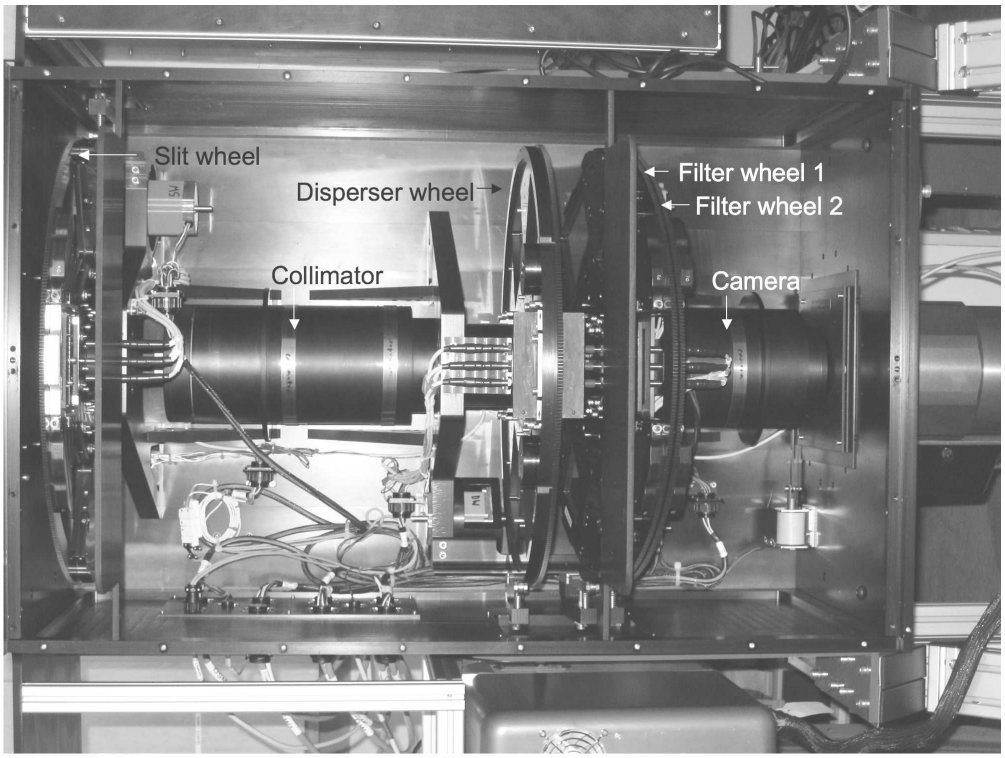

Fig. 7.— Photograph of the internal mechanisms with the top cover removed. Light enters the instrument from the left and the MDM4K is to the right. The four wheels and linear stages are labeled.

The slit wheel positions either long-slits or multi-object slit masks at the location of the telescope focal surface, which is approximately 3 inches from the front of OSMOS. The disperser wheel is located immediately after the collimator lens along the optical path. Finally, there are two filter wheels that are tilted by 8° relative to the optical axis to mitigate ghost reflections. The filter wheels are located in the collimated beam space immediately before the camera lens barrel.

Slits and filters are loaded radially into their respective wheels through hatches in the enclosure that allow ready access for slit or filter exchange while the instrument is mounted on the telescope. These wheels and the aperture cells are nearly identical in that the apertures for both slit and filter cells contain spring-loaded plunger blocks that maintain the position of the cells in the aperture. The cells are held in the wheel in the radial direction with screws. The slit cells have an additional set of spring-loaded plungers that further constrain the cells along the optical axis. Regular exchange of dispersers is not expected because only two of the five available positions for dispersers are presently in use and therefore no special allowance was made to accommodate disperser exchange. Access is obtained with removal of the top panel and the disperser cells are bolted directly into the wheel.

All four of these wheels are driven by a graphite-infused urethane pinion gear bonded to the shaft of a Superior KML062F07 motor. This gear engages a bull gear purchased from Trojon

Gear Inc. on the outer diameter of each wheel and the bull gear blanks were identical for all four wheels. The wheels rotate on a custom turntable bearing from Kaydon. These bearings have two particularly attractive features: 1) they have a very thin (0.25 inch) profile that helps conserve the limited space available in the collimated beam; 2) they deflect very little (less than 1μm) when a force comparable to the weight of the triple prism is applied normal to the wheel plane. This design also allows rapid reconfiguration of the instrument. It takes only a few seconds to change apertures and consequently the instrument can be switched between the imaging and spectroscopy modes in well under ten seconds.

The wheels are held in position by mechanical detents that engage indentations along their outer diameter. Each detent is comprised of a spring-loaded tangent arm carrying a bearing that kinematically docks the wheel in a V-notch at the location of an aperture. The wheel is driven into position with the motor and then the motor is switched off when the wheel reaches the correct location. The wheel is then free to move and the detent spring backdrives the wheel into position. When the detent is engaged in a V-notch, the bearing rests only on two tangent points. An advantage of this approach is that the exact wheel position at each aperture is set by the detent and not the motor. Lab measurements showed that the detent can repeatably back-drive the bearing into the V-notch with better than 1μm precision. A photograph of the detents for the disperser wheel and two filter wheels is shown as Figure 8.

Each aperture position in the wheel is encoded with its position number in binary with a series of three steel pins. An additional pin at each aperture registers when the wheel is in a valid position. These pins are read by inductive proximity sensors manufactured by Pepperl+Fuchs. The advantage of the position encoding is that the motor controllers do not need to remember previous moves in order to determine the current position. This arrangement is also robust against power or communications interruptions.

The wheel position is maintained by the torque produced by the detent, which was designed to be approximately a factor of three greater than the sum of other, "parasitic" torques that would move the wheel out of position. One of these parasitic torques is the motor cogging torque, which is the motor torque when the motor current is off. Other, parasitic torques are the drag torque of the wheel, which is dominated by friction in the turntable bearing, and torques introduced by imbalances in the wheel load.

3.2. Lens Barrel Mounts and Focus

The collimator and camera lens barrels are mounted in V-blocks that determine their relative centration and parallelism along the optical axis. Each barrel is held in its V-block with a pair spring-loaded straps that provide 5g of force. A single bolt with a spherical washer is employed to constrain the location of each lens barrel along the optical axis.

The V-blocks are attached to linear stage mechanisms that move the lens barrels along the

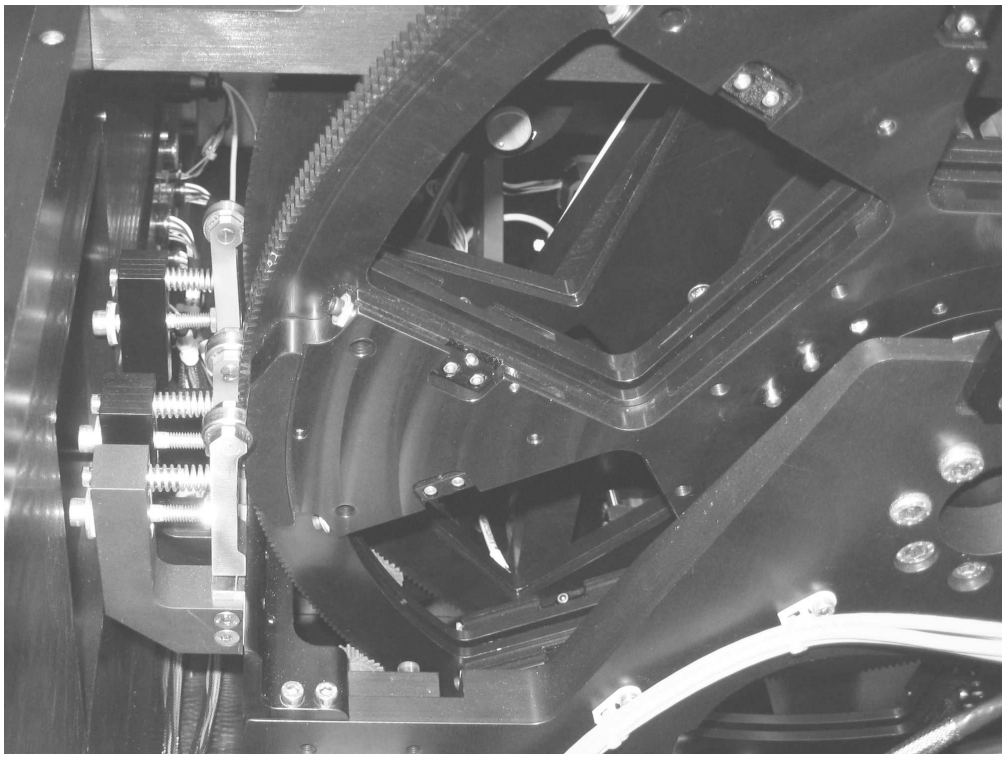

Fig. 8.— Photograph of the spring-loaded detents for the two filter wheels (front) and disperser wheel (back). In all cases the detent is engaged in the wheel. The bull gears on the outer diameter of the filter wheels are also visible.

optical axis for focus. Each linear stage consists of a THK KR3306B+200L0-1000 linear actuator with a 6mm screw pitch that is driven by an Applied Motion HT 17-075-D stepper motor. The motor has 200 steps per revolution and is coupled to a linear actuator with a 1:100 harmonic reducer. One step of the motor consequently corresponds to 0.3μm of focus motion. A pair of Pepperl+Fuchs inductive proximity sensors limit the range of motion of each linear stage. One of these proximity sensors is designated as the home position and the stage position is measured in microns relative to this sensor. The absolute uncertainty in the stage position is dominated by repeatability of the position at which this sensor asserts. We measured the repeatability of the sensor to be approximately 1.5μm, which is much smaller than the camera depth of focus.

The stage position is recorded by the motor controller as the number of motor steps since the last time the stage encountered the home limit. Because the stage position is not indexed or otherwise encoded, a power cycle will erase this relative position information and the relative stage position will need to be reset by moving the stage to the home position. This reset requires approximately 10 seconds.

As in the case of the aperture wheels, the motors that move the linear stages are turned off once a move is complete. Unlike the aperture wheels, however, the stages are not held in position

by a separate mechanical assembly (e.g. a detent). Instead they are effectively held in place by the motor cogging torque, which is amplified by the harmonic reducer. Even when the instrument is pointed at the zenith, and as a consequence the weight of the optics is parallel to the screw of the linear stage, the cogging torque is greater than the torque produced by the weight of the optics against the pitch angle of the slide. There are some additional, less important effects as well, most notably the efficiency of the harmonic reducer and the linear slide.

3.3. Optical Bench

The optical bench is constructed from a 0.5−inch thick 6061 Aluminum plate. The aperture wheels and linear stages are bolted to this plate and their positions are set with precision pins. These pins are sufficient for the optical alignment of the collimator and camera lens barrels, as well as the aperture wheel supports. The stiffness of the optical bench is reinforced with a series of three braces, as well as additional support from the rectangular panels that form the instrument enclosure. The enclosure was designed to allow easy removal of the side and top panels for access to the optical bench, even on the instrument cart, without removal of the entrance and exit plates (which connect to the telescope and Dewar, respectively). The enclosure panels are also constructed of 6061 Al and are bolted together. Finite element analysis of the enclosure indicates that the enclosure is quite stiff. The predicted lateral displacement of the exit plate (the approximate location of the detector) relative to the entrance plate is 20μm for a change in gravity load that corresponds to the difference between zenith and horizon pointing. The tilt of the exit plate corresponds to less than 3μm difference between opposite corners of the detector along the optical axis and this is insufficient to produce defocus across the field.

3.4. Long Slits

The dispersers were designed for use with 1″ slits, which corresponds to an approximately 87μm wide slit. We explored several technologies to fabricate precise and smooth slits that were curved to match the telescope focal surface and chose wire electrical discharge machining (wire EDM). Wire EDM is available with wire thicknesses as fine as 0.0007 inches, which is more than adequate to manufacture slits to our requirements. Each slit was machined in a strip of 0.001 inch thick stainless steel shim stock by EWT/3DCNC, Inc. in Rockford, IL. Prior to this step, the shim stock was clamped between a pair of stainless steel plates that had been machined to match the radius of curvature of the telescope's focal surface. Once the slits were cut, we had them coated with the hot black oxide process by Cleveland Black Oxide to minimize reflections. We measured an rms slit width variation of 0.4μm (or 0.5%) for an 0.003 inch wide slit (76μm or 0.9″) with a uniform calibration source in dispersed light. This fabrication technique therefore met our requirements.

3.5. Multi-Slit Masks

We will employ custom electroformed substrates of Nickel-Cobalt alloy for the multi-slit masks. Electroforming was chosen because this technique can produce thin shells (0.1mm) that exactly match the radius of curvature of the telescope focal surface (O'Brien & Eastman 2006). The mask substrates will then be coated with extremely low reflectivity copper oxide. Slits will be cut in this material with a 3-axis laser system, which will be shared with MODS. The slit masks are approximately 100mm in diameter and slits may be placed over the full FOV, although the wavelength range on the detector will be limited near the two edges of the FOV perpendicular to the dispersion direction. Under typical observing conditions, slits could be employed over an area of ~ 175 arcmin^2 with the VPH grism. This could in principle accomodate up to 100 $10''$ long slits, provided that the target density were sufficiently high. As the triple prism is dispersed over a much shorter region of the detector, the available area for slits with full wavelength coverage is approximately 50% larger and two tiers of slits could be employed. We therefore expect that up to 200 slits could be employed with the triple prism.

4. Instrument Control and Electronics

The OSMOS Instrument Electronics Box (IEB) contains the motor controllers, a Comtrol DeviceMaster RTS-8p Ethernet serial-port server, a WAGO Series 750 modular FieldBus controller, a 5-port ethernet hub, several power supplies, a motor interface board, current sensors, and temperature sensors. The IEB is mounted to one side of OSMOS (the right side shown in Figure 9) and all communication to the mechanisms through the IEB is via a single CAT5 cable. A standard mechanism cable is then used for each mechanism and this cable includes power and sensor information. A block diagram of the OSMOS command structure is shown in Figure 10.

4.1. Motor Control

Each of the six mechanisms is operated with a 7 Amp MicroLYNX motor controller (model MX-CS102-701). These are programmable motor controllers that have a number of attractive advantages, such as non-volatile memory and a simple command set. They also have the capacity for expandable I/O. This motor control architecture was copied from MODS for OSMOS to substantially reduce the development time for the electronics and mechanism control software. A total of seven motor controllers are installed in the IEB (six for regular use and one fully-wired spare). The motor controllers are powered with a 65V unregulated power supply.

The appropriate program to control each mechanism is loaded into the non-volatile memory of its motor controller and is consequently unaffected by power cycles. Mechanism control is then accomplished with a simplified set of commands. This operation is more robust against

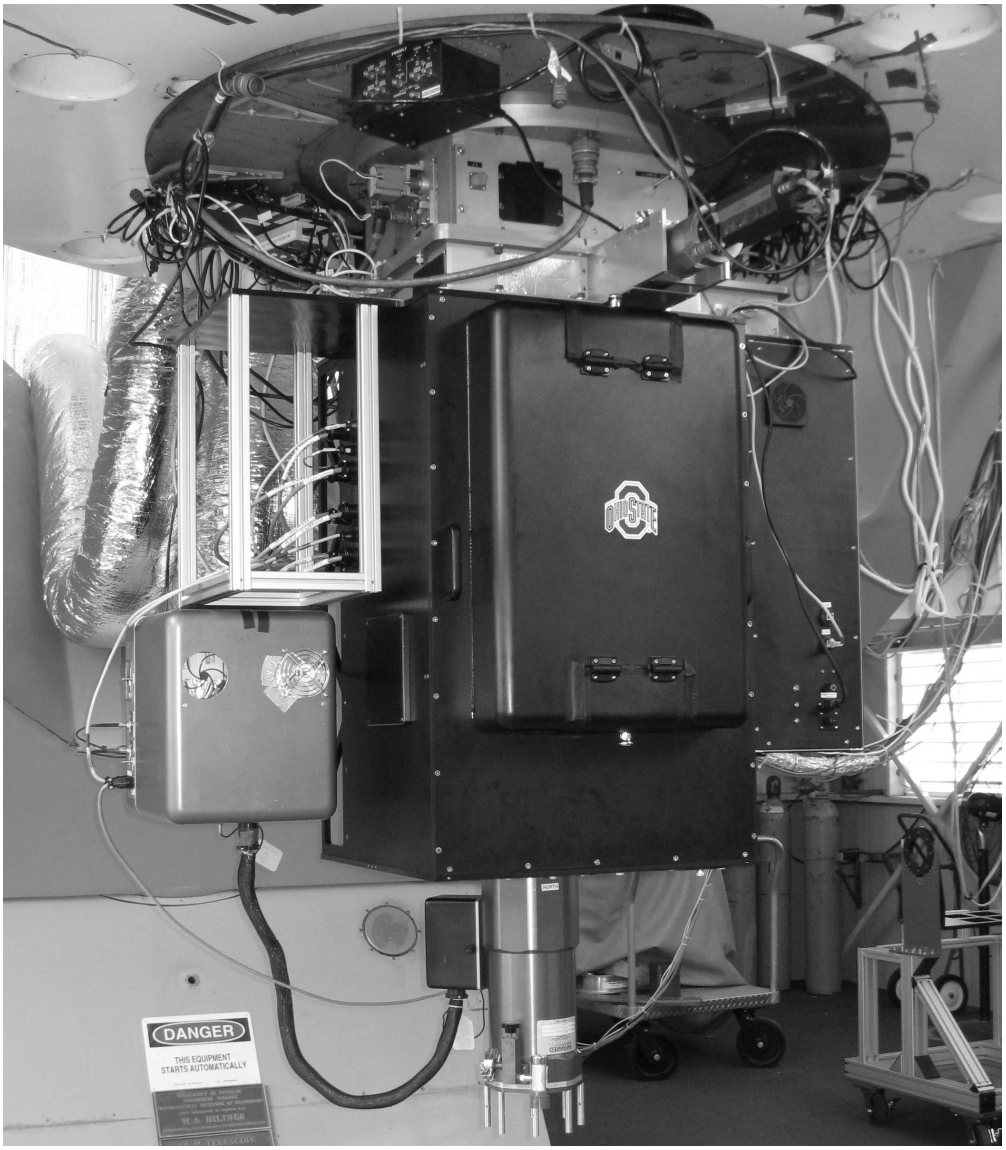

Fig. 9.— OSMOS installed on the 2.4-m Hiltner telescope in April 2010. The top and bottom hatches provide access to the slit wheel and filter wheels, respectively. The IEB is the box mounted to the right of the instrument and the HE is mounted to the left. The cables immediately above the HE are mechanism, a shutter, and temperature cables that connect to the IEB. The MDM4K detector system is immediately below OSMOS.

communication interruptions than a system that requires detailed motor instructions for each move. In addition, the simple command set leads to a substantial reduction in communication latencies.

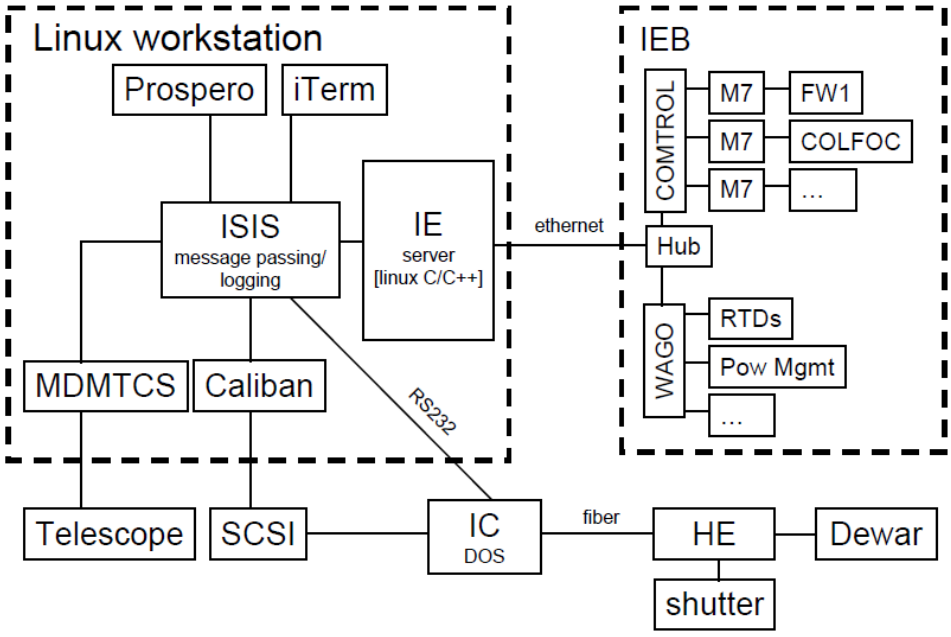

Fig. 10.— Block diagram of the OSMOS control system. The dashed square on the left corresponds to software that runs on the linux workstation used by an observer. Prospero is the observer interface and the iTerm is an engineering interface. ISIS passes commands between Prospero (or the iTerm) and the telescope (MDMTCS), data acquisition system (Caliban), and the Instrument Electronics (IE) server. The IE then issues commands to the IEB. The dashed square on the right delineates representative items within the IEB, such as the MicroLYNX motor controllers (M7). See section 4 for further details.

4.2. System Monitoring

A WAGO modular fieldbus controller with ethernet (model 750-841) is employed to accomplish a range of power switching and system monitoring functions. The WAGO fieldbus was chosen because its wide variety of expansion modules can accomplish all of these functions in a single unit. We use a series of these modules for power switching of individual MicroLYNX controllers and fans, as well as readout of four temperature sensors, and current and voltage sensors for the 65V power supply.

The four temperature sensors are resistance temperature detectors (RTDs) read by a pair of WAGO modules. The RTDs monitor the optical bench, the air inside the instrument, the air inside the dome, and the air inside the IEB. In normal operation all of the motor controllers and power supplies in the IEB are turned on and the total power consumption is 90W. When the mechanisms are in operation, the power consumption rises to approximately 120W. This heat is removed with a circulation fan and an exhaust fan. While these fans can be switched remotely, in normal operation they are continuously in operation. Measurements indicate that these fans maintain the IEB air

temperature at $3-4°$C above ambient. If the fans are turned off, the temperature does not rise sufficiently to damage the electronics.

4.3. Software

The observer interface is the Prospero[4] software package, which was developed in 1995 by R.W. Pogge to control the Imaging Fabry-Perot Spectrograph at the 1.8m Perkins telescope. Prospero has been extensively developed over the years and is presently used to control the OSIRIS (Depoy et al. 1993), TIFKAM (Pogge et al. 1998), ANDICAM (DePoy et al. 2003), DANDICAM, CCDS, MDM4K, and Y4KCAM instruments.

Prospero serves as an interface to the instrument, CCD controller and the MDM Telescope Control Computer (TCS). Prospero communicates with these three clients via the ISIS daemon, which logs and passes commands with the Ohio State ICIMACS (Instrument Control and IMage ACquisition System, Atwood et al. 1998) messaging protocol version 2.5. All commands that control the instrument are passed via ISIS to the Instrument Electronics (IE) server. This server interprets commands and directs them to the appropriate MicroLYNX motor controller via the Comtrol serial port server. The MicroLYNX in turn sends appropriate instructions to move the motor. ISIS directs other commands to either the TCS or CCD controller, as appropriate.

The CCD is controlled by a dedicated workstation called the Instrument Computer (IC) that shares a SCSI disk with the linux workstation that hosts the other servers. The IC then sends commands to the Head Electronics (HE), which is mounted on the opposite side of the instrument from the IEB. Communication between the IC and the HE is via a fiber optic pair. The HE includes the shutter control board and consequently all actions necessary for image acquisition are controlled by the IC and by extension the HE. Figure 10 also contains a block diagram of all of these software and hardware components.

5. Commissioning Results

OSMOS was commissioned at the 2.4m Hiltner Telescope in April 2010. The commissioning time included approximately a week of instrument characterization prior to first light to allow time to integrate OSMOS with the MDM4K detector. Previous instrument characterization at Ohio State was accomplished with a test camera at Ohio State that was too small to sample the entire field of view (the final focal surface is also curved in the absence of the Dewar window of the MDM 4K). The instrument was then tested on sky for one week and the performance is summarized in

[4]http://www.astronomy.ohio-state.edu/~prospero

the next subsections. Practical details are available via the online OSMOS User's Manual[5].

5.1. Imaging Performance

The image quality was characterized in the MDM lab with a grid of precision pinholes. This pinhole mask was constructed from 29 5μm diameter precision pinholes seated in a slit mask cell that matches the spherical focal surface of the 2.4m telescope. These apertures are sufficiently small to measure the point spread function (PSF) of the optical system. With an SDSS z' filter, the average system PSF is 1.7 pixels (0.46″) FWHM over the central 15′ FOV, while the best image quality is 1.3 pixels (0.35″) FWHM at the center of the field.

Chromatic focal shift was measured with a single, on-axis pinhole with a series of narrow-band filters from 365-1000nm. The best camera focus varies by approximately 100μm over this wavelength range, which is the approximate depth of focus. The best compromise focus position results in better than 1.5 pixels (0.41″) FWHM image quality over this entire wavelength range and represents the polychromatic image quality relevant for spectroscopy on-axis with a single slit. The image quality degrades only modestly off axis. In all cases the measured image quality is in good agreement with the predicted performance shown in Figure 2.

The expected throughput of the collimator and camera optics was 64%, which was estimated from the assumption of 2% anti-reflection coatings on each surface and 22 air-glass interfaces (including the Dewar window). Measurements of photometric standards, combined with assumptions about the CCD quantum efficiency and the reflectivity of the primary and secondary, indicate that the throughput is approximately 20% lower than expected. The discrepancy is likely due to poorer performance of the coatings, particularly at the relatively steep incidence angles of light rays at several surfaces.

5.2. Spectroscopic Performance

The triple prism was employed during the commissioning run to measure the spectroscopic (polychromatic) image quality and total system efficiency as a function of wavelength. Observations of stellar objects demonstrated that the image quality is in good agreement with the polychromatic image quality measurements described in Section 2.1. Spectroscopic acquisitions were accomplished with telescope offsets that placed each target at the known position of the slit. Acquisition was then confirmed with direct images of the target through the slit. A planetary nebula was observed to obtain a wavelength solution for the triple prism and measure the resolution as a function of wavelength. These observations showed that the system has good performance from about 380–

[5]http://www.astronomy.ohio-state.edu/~martini/osmos/

1000nm and the resolution of the triple prism varies from $R = 400$ at 400nm to $R = 60$ at 1000nm with an $0.9''$ wide slit (see Figure 4).

As a demonstration of the efficiency of the triple prism, we observed the $z = 6.43$ QSO SDSS J114816.64+525150.3 discovered by Fan et al. (2003). This QSO was initially selected for spectroscopy due to its extremely red $(i - z) = 3.29$ mag color in SDSS photometry. While this extremely faint $i = 23.30$ mag QSO was difficult to precisely align on the spectroscopic slit (because we did not have a z filter), we were able to clearly detect the Lyα emission line at $\sim$ 900nm in approximately ten minutes. Figure 11 shows a 40 minute exposure of this QSO with the triple prism.

The first VPH grism was installed in OSMOS in May 2010. This grism was designed to produce $R = 1600$ with a $1''$ wide slit at have peak diffraction efficiency at $\lambda_B = 450$nm (see §2.2 for further details). Preliminary measurements indicate that it meets all of the design specifications.

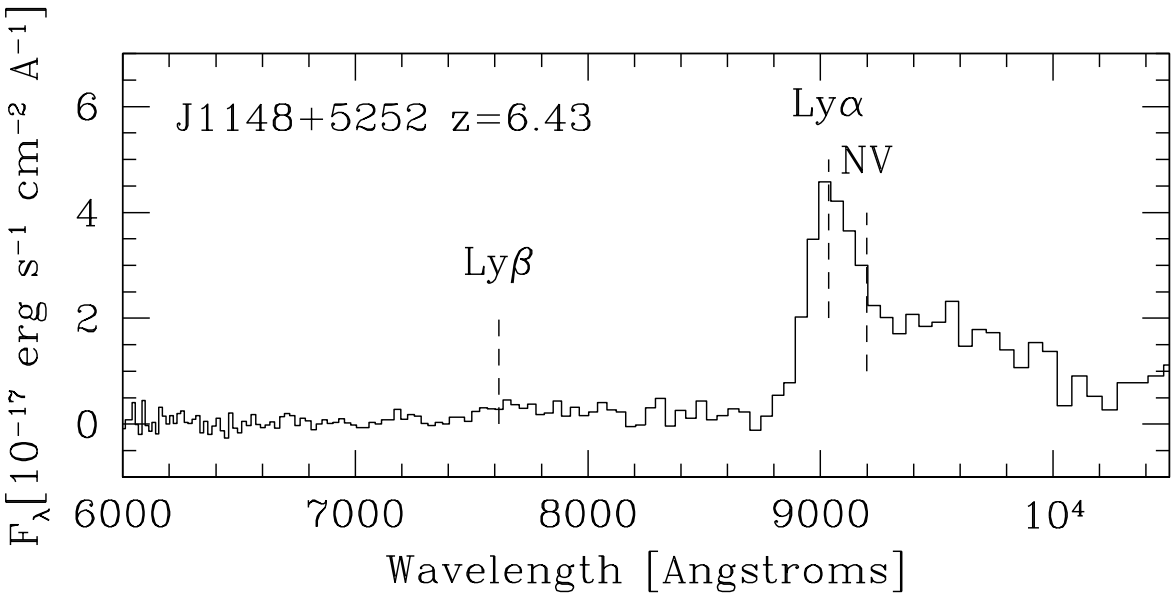

Fig. 11.— Spectrum of the $z = 6.4$ QSO SDSS J114816.64+525150.3 obtained with the triple prism. The QSO has $z_{AB} = 20$ mag and the total integration time is 40 minutes.

5.3. Mechanical Performance

The repeatability and stability of the instrument was measured with the pinhole mask described above. This mask was illuminated by calibration lamps in the MIS and the mechanical flexure and repeatability of the slit wheel and disperser wheel were measured at five telescope positions: zenith, 60° north, 60° south, 4 hours east, and 4 hours west. The instrument was mounted on the telescope

such that the optical bench was oriented E-W. Figure 12 indicates the positions of the pinholes at each of the four cardinal positions relative to zenith. The motion 4 hours east and west (parallel to the optical bench) relative to zenith is approximately 4 pixels, or the equivalent of an average of 1 pixel (0.273″) per hour. The displacement is approximately half this amount perpendicular to the optical bench (north and south). The cluster of points at each position correspond to the individual measurements of the 29 pinholes.

We also determined the mechanical repeatability of the slit wheel mechanism with measurements of the pinhole positions at zenith after several complete revolutions of the slit wheel. The results of this test demonstrated that the repeatability is better than 0.1 pixels (1.5μm or 0.03″). We repeated measurements at zenith after offsets to the four cardinal positions above and the pinhole images were within 0.1 pixels of their initial position. This indicates that the hysteresis is small.

The spectral dispersion direction is perpendicular to the optical bench and this direction was empirically determined to have greater stiffness. We measured the motion of spectral lines at each of the four cardinal positions described above and observed $\sim$ 0.25 pixels of motion when the telescope was offset E and W, or $\sim$ 0.06 pixels per hour. The motion was greater perpendicular to the optical bench (north and south). This motion is shown in Figure 13. The motion perpendicular to the bench in all four directions is comparable to that shown in Figure 12, which indicates that the disperser wheel does not appreciably degrade the performance. We also measured the repeatability of the wavelength solution with a measurement of the wavelength zeropoint both immediately after the telescope offset and after one complete revolution of the disperser wheel. These are shown as the small and large symbols in the panel and demonstrate that the repeatability is excellent.

6. Future Plans

Several observers have now used OSMOS as both an imager and long-slit spectrograph, including for queue-scheduled time that accommodated multiple programs in a single telescope block. In the near future we hope to commission the multi-object capability. The multi-object mode has not yet been commissioned because the present control system for the telescope's instrument rotator is not computer controlled and is insufficiently precise for mask alignment. A plan to upgrade the instrument rotator, its encoder, and integrate rotator control into the telescope control system is presently under development.

Another upgrade to the instrument will be the installation of an extremely red-sensitive, deep-depletion CCD acquired from Lawrence Berkeley National Laboratory (e.g. Roe et al. 2007). This device has higher quantum efficiency above 700nm than the present MDM4K CCD and exhibits minimal fringing, although does also have a substantially higher cosmic ray detection rate. The device we have purchased has 4096x4096 15μm pixels and consequently would have the same plate scale as the present MDM4K detector system. The CCD controller and mount for this detector are

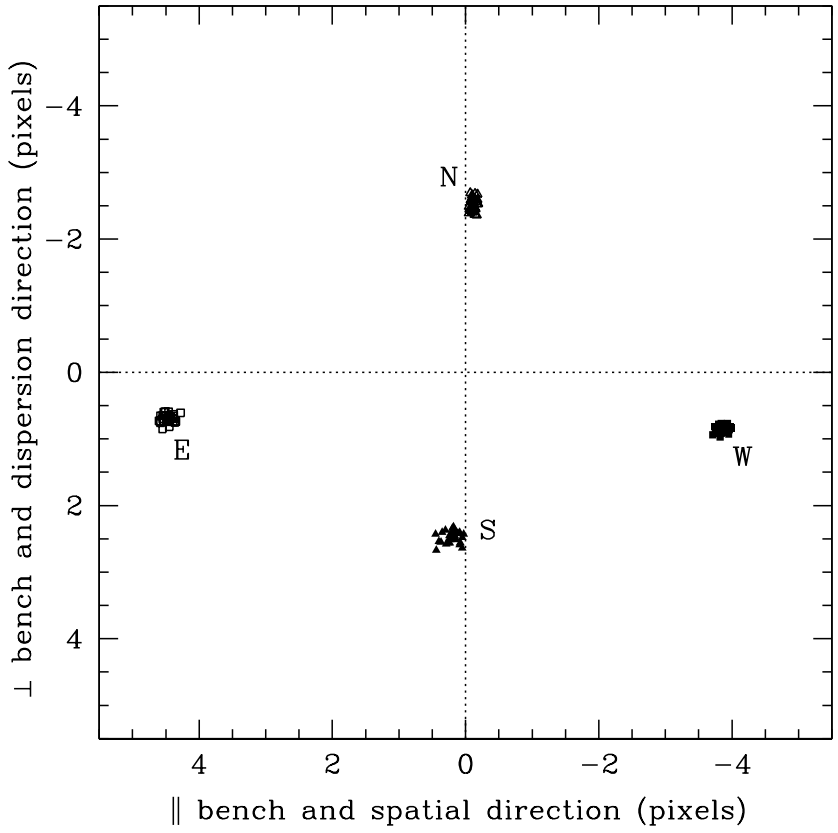

Fig. 12.— Pinhole mask deflection relative to the zenith measured perpendicular and parallel to the optical bench in pixels. One pixel corresponds to 15μm or 0.273″. Measurements were obtained with the telescope 60° north and south (N and S labels) and 4 hours east and west (E and W labels) of the zenith. The intersection of the horizontal and vertical dotted lines corresponds to no deflection. Note that the E and W deflections also exhibit some deflection perpendicular to the bench because the telescope was positioned 4 hours east and west of zenith, not 60° due east and west.

presently under construction. Once complete, observers could request either the more blue-sensitive MDM4K or the more red-sensitive LBNL device.

We are grateful to Marla Geha and Harland Epps for information about the WFCCD optical design and Roberto Tighe and Steve Heathcote for information about Sylgard 184. We thank Frank Pfefferkorn for helpful discussions about manufacturing technologies for the long slits. We also acknowledge numerous helpful comments from the referee that have improved this presentation. OSMOS has been generously funded by the National Science Foundation (AST-0705170) and the Center for Cosmology and AstroParticle Physics at The Ohio State University. Additional support

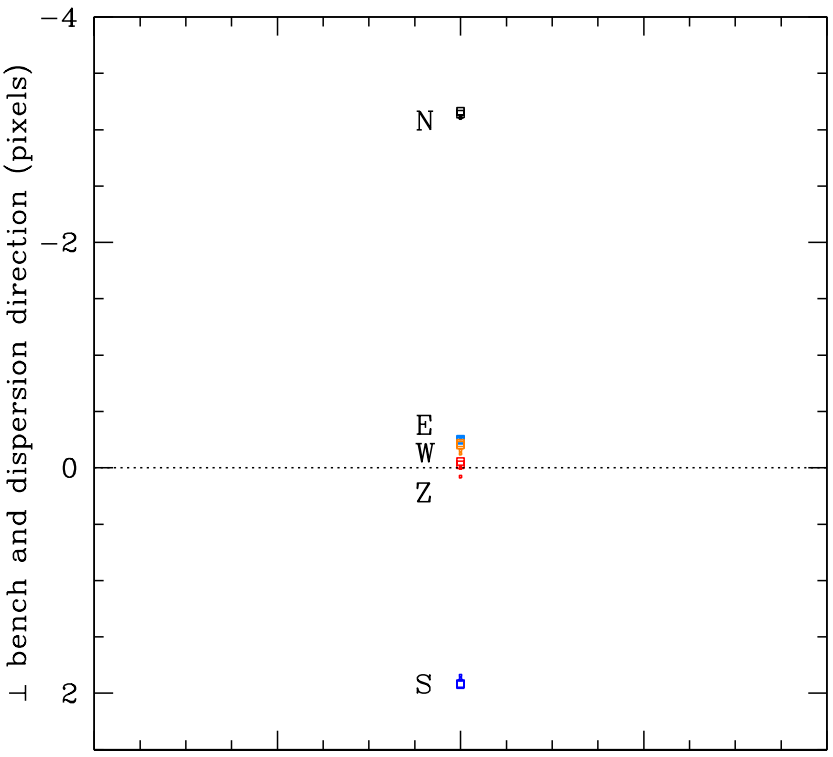

Fig. 13.— Deflection in the dispersion direction measured with the triple prism for the same four positions shown in Figure 12. The spectroscopic slit is oriented E-W (parallel to the optical bench). Measurements were obtained both immediately after offsetting the telescope (*small points*) and after one complete revolution of the disperser wheel (*large points*). The horizontal, dotted line corresponds to the measured position at zenith.

has also been provided by the Department of Astronomy at The Ohio State University and the Department of Physics and Astronomy at Ohio University.

Facilities: Hiltner (OSMOS)

REFERENCES

Atwood, B., Mason, J. A., Duemmel, K. R., O'Brien, T. P., Pogge, R. W., Pappalardo, D., & Hartung, B. 1998, Proc. SPIE, 3355, 560

Barden, S. C., Arns, J. A., Colburn, W. S., & Williams, J. B. 2000, PASP, 112, 809

Bernstein, R., Shectman, S. A., Gunnels, S. M., Mochnacki, S., & Athey, A. E. 2003, Proc. SPIE, 4841, 1694

Depoy, D. L., Atwood, B., Byard, P. L., Frogel, J., & O'Brien, T. P. 1993, Proc. SPIE, 1946, 667

DePoy, D. L., et al. 2003, Proc. SPIE, 4841, 827

Dressler, A. 1980, ApJ, 236, 351

Dressler, A., Lynden-Bell, D., Burstein, D., Davies, R. L., Faber, S. M., Terlevich, R., & Wegner, G. 1987, ApJ, 313, 42

Djorgovski, S., & Davis, M. 1987, ApJ, 313, 59

Fan, X., et al. 2003, AJ, 125, 1649

Martini, P., Kelson, D. D., Kim, E., Mulchaey, J. S., & Athey, A. A. 2006, ApJ, 644, 116

Martini, P., Sivakoff, G.R. & Mulchaey, J.S. 2009, ApJ, 701, 66

Morgan, C. W., Kochanek, C. S., Morgan, N. D., & Falco, E. E. 2006, ApJ, 647, 874

O'Brien, T. P., & Eastman, J. D. 2006, Proc. SPIE, 6273, 89

Peterson, B. M., et al. 2004, ApJ, 613, 682

Pogge, R. W., et al. 1998, Proc. SPIE, 3354, 414

Pogge, R. W., et al. 2006, Proc. SPIE, 6269, 16

Roe, N. A., et al. 2007, Nuclear Instruments and Methods in Physics Research A, 572, 526

Stanek, K. Z., et al. 2003, ApJ, 591, L17

Stoll, R. A., et al. 2010, Proc. SPIE, 7735, 165

Uomoto, A., et al. 1999, Bulletin of the American Astronomical Society, 31, 1501

Zabludoff, A. I., & Mulchaey, J. S. 1998, ApJ, 496, 39